Journal of Sound and Vibration 329 (2010) 3121–3136

Contents lists available at ScienceDirect

Journal of Sound and Vibration

journal homepage: www.elsevier.com/locate/jsvi

Modeling and study of dynamic performance of a valveless micropump

M.N. Hamdan [a,*], S. Abdallah [b], A. Al-Qaisia [c]

[a] Mechanical Engineering Department University of Jordan Amman, Jordan
[b] Mechanical & Aerospace Engineering University of Cincinnati, OH, USA
[c] Mechanical Engineering Department University of Jordan Amman, Jordan

ARTICLE INFO

Article history:
Received 11 November 2009
Received in revised form
28 January 2010
Accepted 29 January 2010
Handling editor: Dr. H. Ouyang
Available online 12 March 2010

ABSTRACT

This work presents an approximate nonlinear analytical model for the problem of fluid–structural interaction in a valveless micropump. The model is constructed using the lumped-mass approach and takes into account the inertial force and time variation of mass density of the working fluid within the micropump chamber, pressure viscous losses of the flow through the diffuser/nozzle elements and the structural geometric nonlinearity due to the membrane mid-plane stretching. It consists of a set of coupled partial integro-differential equations which is reduced to a third order nonlinear coupled fluid-plate vibration equation by using the assumed mode method to approximate the plate dynamic deflection. An approximate analytical solution for the nonlinear vibration model is carried out using the harmonic balance method and is used to investigate the effect of various system parameters on the performance of the micropump. The obtained model and approximate analytical results are compared with those available in the open literature. The approximate analytical results show that, depending on the micropump physical parameters and membrane driving frequency, the working fluid stiffness, which arise in the present model as a result of taking into account the variation of the fluid density with time, and the membrane geometric nonlinearity can have significant effects on the predicted micropump performance and can lead to a complex nonlinear dynamic behavior. The accuracy of these results is subject to a future numerical validation of the presented approximate theoretical model.

1. Introduction

The assessment of dynamic performance of micro-fluid handling devices have in recent years become a major area of research because of very promising technical and commercial potentials of using these devices in the medical as well as in other fields. Advances of microelectromechanical systems (MEMS) manufacturing technology in recent years have enabled the design and fabrication of a variety of miniaturized fluid delivery devices to be used, for example, in controlled drug delivery processes. The practical use of such devices usually involves the design of a controller which requires a good understanding of the device dynamic behavior over a range of operating conditions.

* Corresponding author.
E-mail addresses: mnader@ju.edu.jo (M.N. Hamdan), Shaaban.Abdallah@uc.edu (S. Abdallah), Alqaisai@ju.edu.jo (A. Al-Qaisia).

0022-460X/$ - see front matter © 2010 Elsevier Ltd. All rights reserved.
doi:10.1016/j.jsv.2010.01.035

A main part of a microfluid handling device is the micropump. Over the past two decades a variety of micropump novel designs based on various pumping principles and employing different actuation methods have been proposed for various micro-fluid handling applications [1]. A particular type of micropump which has received a lot of attention in recent years is the diaphragm based-valveless one shown schematically in Fig. 1, [2]. The principles of operation of this type of micropumps are described in [3,4], among others. The vibrating diaphragm constitutes the pumping mechanism, and among the different methods which may be used to actuate this vibration the piezoelectric method is the more commonly used one. This type of micropump design exploits the dependence of pressure loss of the flow through the pair of passive (fixed geometry) diffuser/nozzle elements at the chamber inlet and outlet ports on the direction of the flow through these elements to obtain a one way net flow over a cycle of diaphragm vibration. During the pumping phase, e.g. when the diaphragm is deflected in downward direction, the flow from the pumping chamber is in the nozzle direction at the inlet port and is in the diffuser direction at the output port. On the other hand, during the intake phase of a pumping cycle, e.g. when the diaphragm is deflected upward, the flow through the inlet port is in the diffuser direction and the flow through the output port is in the nozzle direction. Because, with diffuser/nozzle elements having same size and shape, the resistance to flow in the nozzle direction is higher than that in the diffuser direction a net flow from inlet to outlet is obtained over a pumping cycle.

In addition to design simplicity and low production cost this type of micropumps, unlike other type of micropumps, has no interior moving mechanical parts (e.g., check valves) to control pumping chamber inlet and outlet port resistance to flow and thus requires relatively less control effort, has lower risk of clogging and can be driven at higher frequencies than other types of micropumps. These features make this type of micropump attractive in a number of important applications. And, in order to advance their growing use and commercialization, a number of experimental and theoretical investigations of their performance over different ranges of their working and design parameters to improve their performance were carried out, e.g. [5–19].

It is noted that a rigorous study of the dynamic behavior of the whole membrane based-valveless micropump involves formulating and solving highly nonlinear partial differential equations that account for the effects of couplings among various physical fields, e.g., electrical, mechanical, structural and thermal fields. Even when the thermal effects, electro-mechanical field coupling and the geometric non-linearity due to mid-plane stretching are ignored, the dynamic behavior, due to the inherently nonlinear fluid flow equations, of the couple structural–fluid field problem is governed by nonlinear partial differential equations which can only be completely analyzed using cumbersome and time consuming numerical simulation tools. However, numerical results are in general not sufficiently enlightening and approximate analytic solutions are more preferred and needed to guide and verify numerical solutions but are more difficult to obtain. Also the approximate analytical solutions, which can only be obtained after making simplifying assumptions, yield functional relations between system response and parameters and thus give more insight than the numerical ones into the problem underlying physical mechanisms.

Because the problem of obtaining a complete model for the micropump is, as noted above, not at all trivial, various studies have employed different approximate analytical and numerical methods to gain a better understanding of the dynamics of the whole or components of the micropump. Examples of analytical, numerical and experimental studies which have focused on the pressure drop characteristics and rectification of the flow though the diffuser/nozzle elements are found in [5–12]. Approximate theoretical and numerical studies of the dynamics of the flow throughout the micropump, membrane and the actuating piezoelectric or electrostatic field dynamics, have been carried out in [13–19]. These studies have used various simplifying assumptions concerning the effects of fluid–structural and electro-mechanical

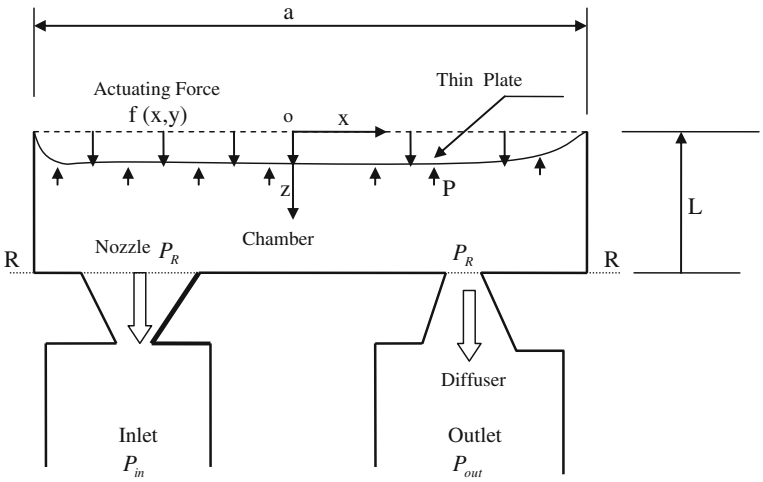

Fig. 1. Schematic representation of the valveless micropump vertical cross section in supply mode.

couplings on the micropump dynamic performance. Cui et al. [13] used an FE software ANSYS to model and simulate the dynamic performance of a valveless micropump excited by a circular piezoelectric-elastic membrane actuator. Their analysis, which is based on mass conservation, accounts for electro-solid–fluid coupling, and the variation of pressure within the micropump chamber due to the unsteadiness of the flow within the chamber, but ignored chamber flow inertial effects and membrane structural nonlinearities. Ng et al. [14] used the boundary element method (BEM) in combination with the finite element method (FET) to study the effect of electro-mechanical coupling on the dynamic response of a micropump driven by an electrostatic actuator. They used von Karman strains to account for mid-plane stretching geometric nonlinearity of the 2-D electrode plate, but ignored fluid–structural interaction effects. Olsson et al. [15] used a lumped-mass approach in conjunction with an FE software ANSYS to construct an analogous four components electrical diagram for the four components (two diffuser/nozzle, chamber and piezoelectric-membrane disc) of a valveless micropump. They employed mass conservation law on the chamber volume, energy equation for diffuser/nozzle/flows and the Newton's second law along with the FE method for the membrane/piezoelectric disc to formulate a four equations dynamic model and analogous electrical diagram for the whole micropump. It is noted that this model accounts for the variation with time of pressure (e.g. variation of mass density) of the flow within the micropump chamber. Accordingly the analogous electrical diagram included a capacitor element that models the finite stiffness of the fluid within the micropump chamber. Olsson et al. above simplified their model to a set of three coupled equations by assuming the fluid inside the micrpump chamber have negligible inertia and infinite stiffness and then used MATLAB to numerically solve the simplified model. Pan et al. [16] developed a single mode nonlinear structural–fluid coupling vibration model for a micropump driven by a square membrane using linear plate theory, mass conservation equation and diffuser/nozzle pressure drop. The source of the nonlinearity in their single degree of freedom oscillator model is a quadratic damping term which arises entirely due the nonlinear pressure-flow rate characteristics of the pump diffuser/nozzle elements. Also their model which ignores inertial and capacitive effects of the unsteady dynamic flow showed no dependence of any of model parameters on the chamber height and thus excludes the effect of the pump size on the dynamic performance of the pump. Pan et al. above presented simulation results of an approximate first order perturbation solution to their nonlinear oscillator model under harmonic excitation for the case where there is no difference between the inlet and outlet pressures. They presented simulation results which showed that, when the nonlinearity is not negligible, the steady sate response amplitude of this oscillator, unlike that of a harmonically forced linearly damped oscillator, reaches its minimum value when the forcing frequency is near the first natural frequency of the plate. Their results also showed that the maximum response, e.g. maximum plate deflection and the maximum pump volumetric stoke, occur at a forcing frequency way below the plate first natural frequency ω_1. Furthermore as the forcing frequency is increased from a zero value the mean flow rate of the pump, for fixed forcing amplitude and magnitude of the nonlinearity coefficient, increases rapidly to a value that remains nearly constant afterwards at a forcing frequency $\omega^* \approx 0.1\omega_1$; that is, from power consumption point of view, ω^* represents an optimal working frequency. Machauf et al. [17] used a simplified single mode-lumped-mass fluid-plate vibration model which, as the model in [16], ignores the unsteadiness of the dynamic flow within the micropump chamber, to numerically study the dynamic performance of an electrostatically actuated valveless micropump.

Pan et al. [18] extended the analysis they presented earlier in [16] by adding the effect of inertial force of the flows inside the pump chamber and through the diffuser/nozzle elements. They obtained a single mode nonlinear vibration model for the plate which differs from the earlier model in [16] in that it accounts for the size (e.g., height) of the pumping chamber and geometry of the diffuser/nozzle elements. The effects of fluid inertia in their new model appear as an added effective inertia term which includes a parameter that depends on the geometry of the diffuser/nozzle in addition to pump chamber size. They presented simulation results of an approximate first order perturbation solution as in [16] for the case where there is no difference between inlet and outlet pressures and showed that the fluid inertia, depending on system parameters, can have significant effects on the phase shift and amplitude of the plate dynamic response to a harmonic excitation. Their results showed that, unlike those predicted using their earlier model in [16], there exists an optimal forcing frequency ω^* which is lower than the plate first natural frequency at which the phase shift reaches 90° and the micropump net output volumetric flux reaches its maximum. Also these results show that the amplitude of the response reaches its maximum value at forcing frequency ω^{**}≠ω^*.

It is noted that the above investigations [16–18] assume the plate (membrane) to be perfectly flat and has uniform, clamped-clamped or simply supported boundary conditions and a linear normal mode dynamic deflection shape. Under these ideal conditions, the plate space-averaged dynamic deflection, which corresponds to the change in pump chamber volume is, except for the first mode, identically zero. Consequently, the obtained volumetric stroke as well as the added inertia due to fluid–structural interaction are, expect for the first linear mode, zero. Fan et al. [19] used finite element method and computational fluid dynamics to simulate the electro-fluid–structural coupling in a piezoelectrically actuated valveless micropump with a clamped rectangular PZT-membrane. They presented numerical results for the case where the PZT-membrane bi-layer first natural frequency is 33.57 kHz. Their results showed that when the excitation frequency is below 7.5 kHz the output flow rate increases and the membrane (plate) deflection shape remains self similar, has a single peak and its amplitude increases as the excitation frequency is increased. However as the excitation frequency exceeds 7.5 kHz the output flow rate and maximum plate deflection tend to decrease and plate deflection tends to exhibit a complicated shape with two or more peaks.

In the present work an approximate nonlinear analytical model for the fluid–structural interaction in a valveless micropump is developed using a lumped-mass approach. The working fluid is assumed to a liquid which has finite

stiffness. The developed model is a set of three nonlinear coupled partial integro–differential equations which account for the inertial force and time variation of mass density of the fluid within the micropump chamber, pressure viscous losses of the flow through the diffuser/nozzle elements and the structural geometric nonlinearity due to the membrane mid-plane stretching. The basic control volume continuity and momentum equations are used to analyze the micropump chamber fluid flow field. The equation of motion that governs the plate transverse dynamic deflection which captures the mid-plane stretching is, for mathematical simplicity, represented by the Berger's approximation [20–22]. In this connection, it is noted that nonlinear vibrations of "dry" elastic plates is an area of active research and there are several analytical and numerical formulations of plate geometric nonlinearity due to mid-plane stretching. The more commonly used plate model is the von Karman model, e.g. [23], but in order to avoid solving two instead of one governing equation, the simpler Berger's model, which assumes the strain energy corresponding to the second invariant of mid-plane strain to be negligible, but nonetheless is known to give reasonably accurate results for the cases of immovable edges [20–22], is instead used in this work. Furthermore, the obtained set of three coupled equations in this work are reduced into a single nonlinear partial integro-differential equation for the fluid-plate vibration by assuming, as in [16,18], the inlet and outlet pressures to be equal. The Galerkin method is then used to obtain a single mode nonlinear temporal model describing the coupled fluid-plate nonlinear vibration which is then solved using the approximate harmonic balance method. The obtained approximate analytical solutions are compared, over a selected range of system parameters, with those obtained numerically and, when it is possible, with those available in [16,18].

2. Problem description

A two dimensional schematic of the vertical cross-section of the diffuser/nozzle micropump under consideration in this work is shown in Fig. 1. The vertical walls and bottom side of the pump chamber, as well as side walls of diffuse/nozzle elements are assumed to be perfectly rigid. The upper part of the chamber is assumed to be an elastic thin plate, which constitutes the pumping mechanism, and is attached firmly to the chamber vertical walls. The chamber, and thus the plate, has a uniform horizontal square cross-section of side length a, and the chamber height is L. The plate is assumed to be isentropic, has mass density ρ_m, uniform thickness h, modulus of elasticity E, and Poisson ratio μ. The actuator, not shown, is assumed to exert an excitation force $f(x,t)$ on the plate upper surface. The dynamic pressure of the fluid in the chamber is assumed to change spatially only with vertical position z, and is given by P at the chamber upper section (e.g. at the plate bottom surface) and by P_R at the chamber bottom section R–R. For simplicity, the diffuser/nozzle elements are assumed to have same shape and geometry. Each of these two elements acts as a diffuser when the flow through the element is in the direction of increasing cross-sectional area, and as a nozzle with this flow is the direction of decreasing of the element cross-sectional area. The inlet pressure is designated by P_{in} and the outlet pressure by P_{out}. The pressures P, P_R, P_{in} and P_{out} are all gauge pressures. The fluid is assumed to have mass density ρ_f which is spatially uniform but is time dependent. During the supply phase of a pumping cycle, e.g. when the plate velocity is in the downward direction, the flow from the chamber through the input port is in the nozzle direction while the flow from the chamber through the output port is in the diffuser direction. During the intake phase, e.g. when the plate velocity is in the upward direction, the flow into the chamber through the input port is in the diffuser direction while the flow from the outlet port into the chamber is in the nozzle direction.

As indicated before, because resistance to flow (e.g. pressure loss) in the nozzle direction is higher than that in the diffuser direction a net flow from inlet to outlet port is obtained over a cycle of plate vibration. Therefore, the formulation of the equations of motion for the flow field requires that one writes the equations for each of the two phases of the pumping cycle and then, under the assumption of same shape and size diffuser/nozzle elements, one combines them into a single set, e.g. [8,11,16–18], that accounts for the dependence of the pressure drop on the direction of the flow velocity.

3. Equations of motions

3.1. Plate model

The equation governing the dynamic deflection of the above described thin, isotropic plate of the micropump, which accounts for the in-plane membrane force, is, using the approximate Berger's plate model, given by [20–22]

$$D\nabla^4 w - N\nabla^2 w + \rho_P \frac{\partial^2 w}{\partial t^2} = f(x,t) - P \tag{1}$$

where $w(x, y, t)$ is the transverse plate deflection (in the z direction),

$$D = \frac{Eh^3}{12(1-\mu^2)}$$

is the plate bending rigidity,

$$\nabla^4 = \frac{\partial^4}{\partial x^4} + 2\frac{\partial^4}{\partial x^2 \partial y^2} + \frac{\partial^4}{\partial y^4}$$

is the bi-harmonic operator,

$$\nabla^2 = \frac{\partial^2}{\partial x^2} + \frac{\partial^2}{\partial y^2}$$

is the Laplacian operator, and N is the induced in-plane membrane force. For cases where the square plate is fastened at its edges in a way that these edges remain at fixed distances apart, N is given by the approximate expression [22],

$$N = -\frac{Eh}{2A_p(1-\mu^2)} \int_0^a \int_0^a w\nabla^2 w \, dx \, dy \tag{2}$$

where $A_p = a^2$ is the un-deformed plate cross-sectional area in the x–y plane.

It is noted that the dynamic pressure P in Eq. (1) is a function of plate defection w and flow field velocity. Thus Eq. (1) must be solved simultaneously with the governing flow field equations. In order to avoid such a complex task of solving simultaneously complicated coupled continuous field equations which can only be done using numerical simulation methods, an approximate analytical solutions for the pressure P and output flow flux are obtained using an approximate lumped parameter analysis of the flow field equations as was done in, e.g., [15–18]. Also, as indicated in the previous section, it is necessary to solve the flow field equations for both the supply and intake phases of the pumping cycle.

3.2. Flow field model

3.2.1. Supply phase, $p > p_{in}$, $p > p_{out}$

Referring to Fig. 1 and to the assumptions stated in Section 2, the application of the momentum equation (e.g. Newton's second law) for the fluid inside the pumping chamber boundaries assuming zero wall shear and negligible momentum flux through the diffuser/nozzle elements, yields [18]

$$P - P_R = P_c = \rho_f A_P \frac{d^2\overline{w}(t)}{dt^2} \tag{3}$$

where

$$\overline{w}(t) = \frac{1}{A_P} \int_a \int w(x, y, t) \, dx \, dy \tag{4}$$

is the plate instantaneous average deflection and P–P_R is, for mathematical convenience, defined as P_c. The diffuser/nozzle elements at inlet and outlet are modeled as passive (fixed geometry) resistive elements. For this phase, where the flow through the chamber inlet port Q_i is in the nozzle direction and that through the outlet port Q_o is in the diffuser direction, the viscous pressure losses thorough these two elements may be expressed as, [15–18],

$$P_R - P_{in} = \rho_f C_n \frac{Q_i^2}{2A^2} \tag{5}$$

$$P_R - P_{out} = \rho_f C_d \frac{Q_o^2}{2A^2} \tag{6}$$

where A is the diffuser(nozzle) throat cross-sectional area, Q_i and Q_o are, respectively, the volumetric fluxes through the inlet and outlet ports of the micropump, and C_d and C_n, ($C_n > C_d$), are, respectively, the diffuser and nozzle pressure loss coefficients. For analysis convenience Eq. (5) is subtracted from Eq. (6) whereby one obtains

$$P_{out} - P_{in} = \frac{C_n \rho_f}{2A^2} Q_i^2 - \frac{C_d \rho_f}{2A^2} Q_o^2 \tag{7}$$

For the special case where $P_{in} = P_{out}$ the above Eq. (7) gives

$$Q_i^2 = \frac{C_d}{C_n} Q_0^2 \tag{8}$$

Next, application of the mass continuity equation for the flow field within the pump chamber, and, for convenience, taking the values of Q_i and Q_o to be negative when flow is out of the pump chamber, yields

$$-\rho_i Q_i - \rho_o Q_o = \frac{d(\rho_c V)}{dt} \tag{9}$$

where V is the instantaneous volume of the micropump chamber, ρ_i, ρ_o and ρc are, respectively, the densities of fluid at inlet, outlet and inside the micropump chamber. Assuming the fluid density to be constant throughout the micropump volume, i.e., let $\rho_i \cong \rho_o \cong \rho_c \equiv \rho_f$, and expressing the chamber volume as $V(t) = V_c + \Delta V(t)$, where $V_c = A_p L$ is the chamber

volume when the plate is flat (e.g., when w=0) and $\Delta V(t) = -A_P\overline{w}(t)$ is the volumetric displacement of the pumping mechanism (plate), Eq. (9) becomes

$$Q_i + Q_o = -\frac{A_P L}{\rho_f}\frac{d\rho_f}{dt} + A_P\frac{d\overline{w}}{dt} \tag{10}$$

It is noted that although the density of the fluid is assumed to be independent of space, which is reasonable considering the small size of the pump control volume, its time variation is not necessarily negligible. Assuming the working fluid stiffness to be finite and using the relation

$$\frac{d\rho_f}{dt} = \frac{\rho_f}{\beta}\frac{dP_c}{dt},$$

where β is the fluid (liquid) isothermal bulk modulus of elasticity coefficient, Eq. (10) becomes

$$Q_i + Q_o = -\frac{A_P L}{\beta}\frac{d(P_c)}{dt} + A_P\frac{d\overline{w}}{dt}. \tag{11}$$

It is noted that because no control valves are present at the inlet and outlet ports of the present micropump the pumping action is mostly hydrokinetic (e.g. the inlet and outlet ports are hydrodynamically connected). Thus the working fluid stiffness in this case is not expected to have the same effect as in the case of a totally hydrostatic pump but its effect will depend among others, on the resistance to flow through the inlet and outlet ports (e.g. on the minimal cross-sectional area of the inlet and outlet ports) as will be shown in later sections.

Next, solving Eqs. (3)–(7), and (11) simultaneously for P, Q_i, and Q_0 leads to

$$P = \frac{P_{in}+P_{out}}{2} + \frac{C_n\rho_f}{4A^2}Q_i^2 + \frac{C_d\rho_f}{4A^2}Q_o^2 + \rho_f L\frac{d^2\overline{w}}{dt^2} \tag{12}$$

$$Q_i = \frac{-(C_d/C_n)(A_P\dot{\overline{w}} - (A_P L/\beta)\dot{P}_c) + \sqrt{(C_d/C_n)(A_P\dot{\overline{w}} - (A_P L/\beta)\dot{P}_c)^2 + (1-(C_d/C_n))((2A^2/C_d\rho_f)\Delta P)}}{1-(C_d/C_n)} \tag{13}$$

and

$$Q_o = \frac{(A_P\dot{\overline{w}} - (A_P L/\beta)\dot{P}_c) - \sqrt{(C_d/C_n)(A_P\dot{\overline{w}} - (A_P L/\beta)\dot{P}_c)^2 + (1-(C_d/C_n))((2A^2/C_d\rho_f)\Delta P)}}{1-(C_d/C_n)} \tag{14}$$

where $\Delta P = P_{out} - P_{in}$. It is noted that the process of obtaining the above two equations involves solving quadratic equations for Q_i and Q_0. The sign of radicals in these equations are determined by the requirements that Q_i and Q_0 must satisfy Eq. (10) and $Q_0 > Q_i$ for the supply phase.

Eqs. (1)–(3), and (12)–(14) represent the micropump dynamic lumped-mass model for the supply phase. These equations can, for given $f(t)$, P_{in}, P_{out}, and plate deflection mode shape, be used to determine the four unknowns w, Q_i, Q_0 and P_c.

3.2.2. Intake phase: $p < p_{in}$, $p < p_{out}$

The derivation of the governing equations for this phase follows the same procedure used for the supply phase, except that in this case the flows into the chamber are considered positive, and the flow through the inlet port is in the diffuser direction while that through the outlet port in the nozzle direction. Accordingly, the governing equations for the pressure losses through the inlet and outlet ports of the chamber and the mass continuity of the flow field within the chamber take the form

$$P_{in} - P_R = \rho_f C_d\frac{Q_i^2}{2A^2} \tag{15}$$

$$P_{out} - P_R = \rho_f C_n\frac{Q_o^2}{2A^2} \tag{16}$$

and

$$Q_i + Q_o = \frac{A_P L}{\beta}\frac{d(P_c)}{dt} - A_P\frac{d\overline{w}}{dt} \tag{17}$$

Subtracting Eq. (15) from Eq. (16), one obtains

$$P_{out} - P_{in} = \frac{C_n\rho_f}{2A^2}Q_0^2 - \frac{C_d\rho_f}{2A^2}Q_i^2 \tag{18}$$

where for the special case of P_{in}=P_{out} the above equation becomes

$$Q_o^2 = \frac{C_d}{C_n}Q_i^2 \tag{19}$$

Solving simultaneously Eqs. (15)–(17), along with Eq. (3), for P, Q_i and Q_0 leads to

$$P = \frac{P_{in}+P_{out}}{2} - \frac{C_d\rho_f}{4A^2}Q_i^2 - \frac{C_n\rho_f}{4A^2}Q_o^2 + \rho_f L\frac{d^2\overline{w}}{dt^2} \tag{20}$$

$$Q_o = \frac{-(C_d/C_n)((A_PL/\beta)\dot{P}_c - A_P\dot{\overline{w}}) + \sqrt{(C_d/C_n)((A_PL/\beta)\dot{P}_c - A_P\dot{\overline{w}})^2 + (1-(C_d/C_n))((2A^2/\rho_f C_n)\Delta P)}}{1-(C_d/C_n)} \tag{21}$$

and

$$Q_i = \frac{((A_PL/\beta)\dot{P}_c - A_P\dot{\overline{w}}) - \sqrt{(C_d/C_n)((A_PL/\beta)\dot{P}_c - A_P\dot{\overline{w}})^2 + (1-(C_d/C_n))((2A^2/\rho_f C_n)\Delta P)}}{1-(C_d/C_n)} \tag{22}$$

where as before, $\Delta P = P_{out} - P_{in}$ and the sign of radicals in these equations are determined by the requirements that Q_i and Q_0 must satisfy Eq. (17) and $Q_0 < Q_i$ for this phase.

Eqs. (1)–(3), and (20)–(22) represent the micropump dynamic model for the intake phase, e.g. for the case $\dot{\overline{w}} < 0$. These equations can, for given $f(x,t)$, P_{in},P_{out}, and plate deflection mode shape, be used to determine the four unknowns w, Q_i, Q_0, P and P_c during the intake phase.

3.2.3. Combined model

Eqs. (1)–(3), (12)–(14) and (20)–(22), along with Eq. (2) describe the micropump dynamic behavior during the intake and supply phases. This set of equations are, for convenience, rewritten in the following form:

$$D\nabla^4 w - N\nabla^2 w + \rho_P h\frac{\partial^2 w}{\partial t^2} + \rho_f L\frac{d^2\overline{w}}{dt^2} + \frac{\rho_f}{4A^2}R(Q_i,Q_o) = f(x,t) - \frac{P_{in}+P_{out}}{2} \tag{23}$$

where

$$R(Q_i,Q_o) = \begin{cases} C_nQ_i^2 + C_dQ_o^2 & \text{for} \quad \dot{\overline{w}} > 0 \\ -C_dQ_i^2 - C_nQ_o^2 & \text{for} \quad \dot{\overline{w}} < 0 \end{cases}, \tag{24}$$

N is as given in Eq. (2), and Q_i and Q_0 are, respectively, given by Eqs. (13) and (14) when $\dot{\overline{w}} > 0$, and by Eqs. (21) and (22) when $\dot{\overline{w}} < 0$. Eqs. (3)–(24) constitute an approximate partial integro-differential nonlinear model for the present valveless micropump which is not easily analyzed using approximate analytical methods. A simplified form of this model that can be analyzed analytically is presented in the next section.

4. Approximate model

For the special case of $\Delta P = 0$, $P_{in} = 0$ the model obtained above can be reduced to an integro-partial differential equation with single independent variable $\overline{w}$ that can be analyzed, after introducing reasonable simplifications, using approximate analytical methods. Accordingly, for this special case, the flux Eqs. (13), (14), (21)–(24) become:For $\dot{\overline{w}} > 0$

$$Q_o = \frac{A_P\dot{\overline{w}} - (A_PL/\beta)\dot{P}_c}{1+\sqrt{(C_d/C_n)}} \tag{25}$$

$$Q_i = \frac{\sqrt{(C_d/C_n)}\left(A_p\dot{\overline{w}} - (A_PL/\beta)\dot{P}_c\right)}{1+\sqrt{(C_d/C_n)}} = \sqrt{\frac{C_d}{C_n}} \quad Q_o \tag{26}$$

$$R(Q_i,Q_0) = \frac{2C_dC_n[A_p\dot{\overline{w}} - (A_PL/\beta)\dot{P}_c]^2}{(\sqrt{C_d}+\sqrt{C_n})^2} \tag{27}$$

and for $\dot{\overline{w}} < 0$

$$Q_i = \frac{-A_P\dot{\overline{w}} + (A_PL/\beta)\dot{P}_c}{1+\sqrt{(C_d/C_n)}} \tag{28}$$

$$Q_o = \frac{\sqrt{(C_d/C_n)}\left(-A_p\dot{\overline{w}} + (A_PL/\beta)\dot{P}_c\right)}{1+\sqrt{(C_d/C_n)}} = \sqrt{\frac{C_d}{C_n}} \quad Q_i \tag{29}$$

$$R(Q_i,Q_0) = \frac{-2C_dC_n[-A_p\dot{\overline{w}} + (A_PL/\beta)\dot{P}_c]^2}{(\sqrt{C_d}+\sqrt{C_n})^2} \tag{30}$$

Next, using the time derivative of Eq. (3) to rewrite the above expressions of Q_i and Q_0 in terms of $\overline{w}$, one has

$$\dot{P}_c = \frac{L\rho_f}{\beta}\dot{P}_c\ddot{\overline{w}} + \rho_f L\dddot{\overline{w}} \tag{31}$$

Solving the above equation for $\dot{P}_c$ one obtains

$$\dot{P}_c = \frac{L\rho_f\dddot{\overline{w}}}{1-(L\rho_f/\beta)\ddot{\overline{w}}} \tag{32}$$

Then using the small term approximation, (e.g., in most practical cases $(L\rho_f/\beta)\ddot{\overline{w}} \ll 1$), the above equation yields the following approximate expression for $\dot{P}_c$:

$$\dot{P}_c = L\rho_f\dddot{\overline{w}} \tag{33}$$

Substituting Eq. (33) into Eqs. (27) and (30), expanding the square bracketed terms and ignoring the term

$$\left(\frac{A_P\rho_f L^2}{\beta}\dddot{\overline{w}}\right)^2$$

which appears in these expansions, and because the pressure drop is in the direction of flow through the diffuser /nozzle elements, the terms $\ddot{\overline{w}}^2$ and $-\ddot{\overline{w}}\dddot{\overline{w}}$, are rewritten, respectively, as $\ddot{\overline{w}}|\ddot{\overline{w}}|$ and $\ddot{\overline{w}}/\dddot{\overline{w}}$ to allow for reverse flow, leads to

$$R(Q_i,Q_o) = \begin{cases} \dfrac{2C_dC_n\left(A_P^2\ddot{\overline{w}}^2-(2L^2A_P^2/\beta)\ddot{\overline{w}}\dddot{\overline{w}}\right)}{(\sqrt{C_n}+\sqrt{C_d})^2} & \text{for} \quad \ddot{\overline{w}}>0 \\ \dfrac{-2C_dC_n\left(A_P^2\ddot{\overline{w}}^2-(2L^2A_P^2/\beta)\ddot{\overline{w}}\dddot{\overline{w}}\right)}{(\sqrt{C_n}+\sqrt{C_d})^2} & \text{for} \quad \ddot{\overline{w}}<0 \end{cases} = \frac{2C_dC_n\left(A_P^2|\ddot{\overline{w}}|\ddot{\overline{w}}+(2L^2A_P^2/\beta)|\ddot{\overline{w}}|\dddot{\overline{w}}\right)}{(\sqrt{C_n}+\sqrt{C_d}}\Big)^2 \quad \text{for} \quad \text{all} \quad \ddot{\overline{w}} \tag{34}$$

Substituting Eq. (34) into Eq. (23), and Eqs. (25) and (29) into the mean output flux $\overline{Q}$ equation

$$\overline{Q} = \frac{1}{T}\int_0^T Q_o\,dt, \tag{35}$$

where T is the period of the excitation force $f(x,t)$ and using the relation $V_c=A_PL$, then, for the special case of $P_{in}=P_{out}=0$, one obtains the following approximate coupled fluid-plate vibration equation

$$D\nabla^4 w - N\nabla^2 w + \rho_P h\frac{\partial^2 w}{\partial t^2} + \rho_f L\frac{d^2\overline{w}}{dt^2} + \frac{\rho_f A_P^2 C_dC_n}{2A^2(\sqrt{C_d}+\sqrt{C_n})^2}\left(|\ddot{\overline{w}}|\ddot{\overline{w}} + 2\frac{L\rho_f}{\beta}\ddot{\overline{w}}\dddot{\overline{w}}\right) = f(x,t), \tag{36}$$

and the mean output flux $\overline{Q}$ relation

$$\overline{Q} = \frac{A_p}{T(\sqrt{C_n}+\sqrt{C_d})}\int_0^T(\ddot{\overline{w}}-(L^2\rho_f/\beta)\dddot{\overline{w}})[\sqrt{C_n}U(\ddot{\overline{w}})+\sqrt{C_d}U(-\ddot{\overline{w}})]dt \tag{37}$$

where N is as given by Eq. (2), and U, is the unit step function. It is noted that the present model above coincides with that developed by Pan et al. [16] after deleting from it the nonlinear geometric, fluid inertial and fluid stiffness terms (e.g. after setting each term involving N, L and β in Eqs. (36) and (37) to zero). The present model also agrees with that developed by Pan et al. [18] after deleting from the present model the nonlinear geometric term and the fluid stiffness terms (terms involving β) and keeping in Pan et al. model only the inertial effect of the pump chamber flow (e.g. after deleting from Pan et al. model the inertial effect of diffuser/nozzle element flows).

5. Analysis

5.1. Reduced order model

The governing nonlinear spatially continuous coupled fluid-plate vibration Eq. (36) does not admit closed form solutions. Also this equation is not readily amenable to well known approximate analytical methods of the nonlinear theory, such as the perturbation methods, partly because it contains a third order time derivative term. It is noted that a widely used approach for analyses of nonlinear spatially continuous equations is to reduce them to ordinary differential equations in time using a spatial discretization approach, such as the finite element (FE) or the assumed mode methods [23]. In the present work the direct and simple approach of the assumed one-linear-mode method is used to reduce Eq. (36) to a SDOF ordinary differential equation in time. Accordingly one

assumes

$$w_i(x,y,t) = q_i(t) f_i(x,y) \tag{38}$$

where $q_i(t)$ is the ith mode, unspecified function of time generalized coordinate and $\phi_i(x,y)$ is the ith linear mode shape function of the plate in the absence of fluid interaction which satisfies the linear equation

$$\frac{D}{ha^4\rho_P}\nabla^4\phi_i(x,y) = \omega_i^2\phi_i(x,y) \tag{39}$$

where ω_l is the dry plate ith natural frequency. By means of the Galerkin's standard procedure, substituting Eqs. (38), (39) and (2) into Eq. (36), inserting dimensionless variables

$$\xi_1 = \frac{x}{a}, \quad \xi_2 = \frac{y}{a},$$

assuming, without loss of generality, that $f(x,t)$ spatial distribution is given by ϕ_i and is harmonic-in-time, multiplying the outcome by ϕ_i and integrating it from ξ_1,ξ_2=0 to ξ_1,ξ_2=1, and dropping the i subscript for convenience, one obtains the ith mode SDOF reduced coupled fluid-plate vibration model

$$\alpha_1\ddot{\overline{q}} + \alpha_2 q + \alpha_3|\dot{\overline{q}}|\dot{\overline{q}} + \alpha_4 q^3 + \alpha_5|\dot{\overline{q}}|\overline{q} = F^*\sin(\omega t) \tag{40}$$

where

$$\alpha_1 = \int_0^1\int_0^1\phi^2 d\xi_1 d\xi_2 + \frac{L\rho_f}{h\rho_P}(\int_0^1\int_0^1\phi d\xi_1 d\xi_2)^2, \alpha_2 = \omega_p^2\int_0^1\int_0^1\phi^2 d\xi_1 d\xi_2, \alpha_3 = \frac{C_n C_d A_P^2\rho_f}{2hA^2\rho_P(\sqrt{C_n}+\sqrt{C_d})^2}(\int_0^1\int_0^1\phi d\xi_1 d\xi_2)^3,$$

$$\alpha_4 = \frac{E}{2A_P^2\rho_P(1-\mu^2)}[\int_0^1\int_0^1\phi(\phi_{\xi_1\xi_1}+\phi_{\xi_2\xi_2})d\xi_1 d\xi_2]^2, \alpha_5 = \frac{-2L^2\rho_f}{\beta}\alpha_3, F^* = \frac{F_0}{h\rho_P}(\int_0^1\int_0^1\phi^2 d\xi_1 d\xi_2), \tag{41}$$

ω andF_0 are, respectively, the frequency and amplitude of the harmonic excitation, and ω_p is the ith natural frequency of the dry plate corresponding to the ith normal mode $\phi_i \equiv \phi$ used in the above equations. For convenience, Eq. (40) is normalized using the following dimensionless system parameters and variables:

$$\tau = \left(\frac{\alpha_2}{\alpha_1}\right)^{1/2}t, \quad \nu = \frac{q}{h}, \quad b_1 = \frac{A}{A_p}, \quad b_2 = \frac{h}{a}, \quad b_3 = \frac{L}{a}, \quad b_4 = \frac{\rho_f}{\rho_P}, \quad b_5 = \frac{C_d}{C_n}, \quad b_6 = \frac{\beta}{E} \tag{42}$$

Inserting the above dimensionless parameters and variables into Eqs. (40) and (41), noting that the plate area is $A_p = a^2$, and expressing the dry plate natural frequency ω_P as

$$\omega_P = \left(\frac{k^2 D}{a^4\rho_P h}\right)^{1/2},$$

where k is a parameter associated with the used mode shapeϕ leads to the following one-mode non-dimensional coupled fluid-plate vibration model;

$$\ddot{\nu} + \nu + \beta_1|\dot{\nu}|\dot{\nu} + \beta_2\nu^3 + \beta_3|\dot{\nu}|\ddot{\nu} = F\sin(\Omega c\tau) \tag{43}$$

where a dot now represents a derivative with respect to the dimensionless time τ , and

$$\beta_1 = \frac{C_d b_4[\int_0^1\int_0^1\phi d\xi_1 d\xi_2]^3}{2b_1^2(1+\sqrt{b_5})^2}[\int_0^1\int_0^1\phi^2 d\xi_1 d\xi_2 + (b_3 b_4/b_2)[\int_0^1\int_0^1\phi d\xi_1 d\xi_2]^2], \beta_2 = \frac{6}{k^2}\frac{[\int_0^1\int_0^1\phi(\phi_{\xi_1\xi_1}+\phi_{\xi_2\xi_2})d\xi_1 d\xi_2]^2}{\int_0^1\int_0^1\phi^2 d\xi_1 d\xi_2},$$

$$\beta_3 = \frac{C_d k^2 b_2^2 b_3^2 b_4^2}{12(1-\mu^2)(1+\sqrt{b_5}}\Big)^2 b_1^2 b_6\frac{(\int_0^1\int_0^1\phi d\xi_1 d\xi_2)^3(\int_0^1\int_0^1\phi^2 d\xi_1 d\xi_2)}{[\int_0^1\int_0^1\phi^2 d\xi_1 d\xi_2 + (b_3 b_4/b_2)(\int_0^1\int_0^1\phi d\xi_1 d\xi_2)^2]^2},$$

$$F = \frac{F_0}{\rho_P h^2\omega_P^2}, \quad \Omega = \frac{\omega}{\omega_P}, \quad C = \left[\frac{\int_0^1\int_0^1\phi^2 d\xi_1 d\xi_2 + (b_3 b_4/b_2)(\int_0^1\int_0^1\phi d\xi_1 d\xi_2)^2}{\int_0^1\int_0^1\phi^2 d\xi_1 d\xi_2}\right]^{1/2} \tag{44}$$

Also, for convenience, the pump mean output net flux $\overline{Q}$, given by Eq. (37) is rewritten in non-dimensional form using the parameters and variables defined in Eq. (42), whereby one obtains

$$Q = \frac{\Omega(\int_0^1\int_0^1\phi d\xi_1 d\xi_2)}{2\pi(1+\sqrt{b5})}\int_0^T\left[\dot{v} - \frac{b_4 b_3^2 b_2^2 k^2}{12c^2 b_6(1-\mu^2)}\ddot{v}\right]\left(U(\dot{v})+\sqrt{b_5}U(-\dot{v})\right)d\tau \tag{45}$$

where

$$Q = \frac{\overline{Q}}{a^2 h\omega_p} \tag{46}$$

is the micropump non-dimensional output mean flux over a period of excitation $T=(2\pi/\Omega C)$, and $U(\dot{v})$ and $U(-\dot{v})$ are unit step functions each of which is zero when its argument is negative and 1 when its argument is positive. Note that, in the above model, the coefficient β_1 is due to diffuser/nozzle resistance (viscous pressure drop) and flow inertial effects, β_2 is due to geometric nonlinearity induced by in-plane membrane force, while β_3 is due to a combined effect of inertia and finite stiffness of the chamber flow. The case β_3 is zero corresponds to a finitely rigid fluid and Eq. (43) in this case is reduced to a second order nonlinear differential equation. And when also β_2 is set to zero, e.g. when structural nonlinearity is also ignored, Eq. (43) takes the same nonlinear form as that of the valveless micropump one-mode reduced dynamic model presented in [16,18].

It is noted that, as can be seen from Eqs. (43)–(46), the expressions for the micropump mean flux Q and the fluid–structural coupling parameters β_1 and β_3 include the mean modal deflection $\int_0^1\int_0^1\phi d\xi_1 d\xi_2$, or a power multiple of it, of the excited linear mode ϕ of the dry plate vibration as a multiplying factor. Thus for a mode shape ϕ for which this factor is zero, e.g. for a skew symmetrical mode shape, the plate vibration becomes unaffected by the fluid and model in Eq. (43) reduces to that of the nonlinear dry plate. For example for a plate with all edges hinged or fully clamped to rigid supports (also for several other combination of edge-boundary conditions) the $\int_0^1\int_0^1\phi d\xi_1 d\xi_2$ is zero for all modes other than the fundamental one [24,25]. Thus according to the present model, as well as the models developed in [16,18], the micropump mean output flow and the fluid–structural coupling parameters β_1 and β_3 are nonzero only when the plate is vibrating at the fundamental mode: i.e. , the plate modal vibration, according to the present model and the models in [15–18], is affected by the flow field dynamics only when the plate is vibrating at the fundamental mode. Also, according to the present model and the models presented in [16–18], the linear undamped natural frequency ω_n of the coupled fluid-plate modal vibration is given by, (see Eq. (40)),

$$\omega_n = \sqrt{\frac{\alpha_2}{\alpha_1}} = \left[\frac{\omega_p^2\int_0^1\int_0^1\phi^2 d\xi_1 d\xi_2}{\int_0^1\int_0^1\phi^2 d\xi_1 d\xi_2 + \frac{L\rho_f}{h\rho_p}(\int_0^1\int_0^1\phi d\xi_1 d\xi_2)^2}\right]^{1/2} \tag{47}$$

where ω_p is the dry plate undamped natural frequency corresponding to the mode ϕ. It can be seen from this equation that for modes ϕ for which $\int_0^1\int_0^1\phi d\xi_1 d\xi_2 = 0$, e.g. for skew symmetrical normal modes, the dry plate undamped natural frequency coincides with that of wet plate. Also the above equation shows that coupled flow–structural interaction effect on the linear undamped free vibration frequency of the plate appears as an added inertia, while, see Eqs. (43) and (44), this interaction includes both the inertial (added mass) and added stiffness effects on the nonlinear un-damped free vibration frequency of the plate. It is to be noted that the above features of the present coupled fluid-plate vibration model and the models developed in [16–18], are in part be due to using the approximate one-mode method to simplify the continuous model in Eq. (36). However, using, for example, a multi-mode approach, the assumed harmonic-in-time approach or other discretization methods to approximate the continuous model in Eq. (36) may lead to predictions of the micropump behavior different from those discussed above, and, due to a limited scope, are not pursued in this work.

5.2. Approximate analytical solution

The coefficients β_1, β_2 and β_3 in the dimensionless nonlinear reduced single-mode coupled fluid-plate vibration model in Eq. (43), evaluated using Eq. (44) for a selected range of typical micropump physical parameters, show that this vibration model is strongly nonlinear. For example, for a micropump with aluminum square plate with simply supported edge conditions, side length $a=1000\,\mu m$, modulus of elasticity $E=7\times10^{10}\,N/m^2$, mass density $\rho_P=2778\,kg/m^3$, Poisson's ratio $\mu=0.25$, thickness $h=40\,\mu m$, having chamber length $L=500\,\mu m$, diffuser loss coefficient $C_d=1$, nozzle loss coefficient $C_n=1.5$, diffuser/nozzle throat area $10\,\mu m$, working fluid bulk modulus $\beta=1.7\times10^9\,N/m^2$ and fluid mass density $\rho_f=1000\,kg/m^3$, Eq. (44) yields $\beta_1=36.63$, $\beta_2=1.5$ and $\beta_3=3.80$. In addition to the fact that the nonlinear vibration model is, for the range of parameter values considered, not weakly nonlinear, it includes a third order time derivative of the dependent variable and is thus not readily amenable to well known approximate analytical perturbation or averaging methods. In the present work, for the sake of simplicity, an approximate low order steady state solution to this nonlinear vibration problem in Eq. (43) is obtained using the single harmonic balance (SHB) method. For convenience, an unknown constant phase φ is introduced in the excitation so that the fundamental harmonic response contains a single trigonometric term. Accordingly, Eq. (43) is rewritten as

$$\ddot{v} + v + \beta_1|\dot{v}|\dot{v} + \beta_2 v^3 + \beta_3|\dot{v}|\ddot{v} = F\sin(c\Omega\tau+\varphi). \tag{48}$$

Noting that the nonlinear terms in Eq. (47) are symmetric, an approximate SHB solution takes the form [26,27]

$$v(\tau) = A_1 \sin(\Omega c\tau) \tag{49}$$

where A is a constant amplitude. Substituting Eq. (49) and its time derivatives into Eq. (47) and using trigonometric identities, it follows that

$$\left[A(1-c^2\Omega^2)+\frac{3}{4}\beta_2 A^3\right]\sin(c\Omega\tau)+[c^2\Omega^2\beta_1 A^2-c^4\Omega^4\beta_3 A^2]|\cos(c\Omega\tau)|\cos(c\Omega\tau) - \frac{\beta_2 A_1^3}{4}\sin(3c\Omega\tau) = F\sin(c\Omega\tau)\cos(\phi)+F\cos(c\Omega\tau)\sin(\phi) \tag{50}$$

Replacing the nonlinear term $|\cos(c\tau\Omega|\cos(c\Omega\tau)$ in Eq. (50) by a truncated Fourier series expansion and matching the coefficients of $\sin(c\Omega\tau)$ and the coefficients of $\cos(c\Omega\tau)$ in the resulting equation, (or equivalently, multiply Eq. (50) by $\sin(c\Omega\tau)$ and integrate it over one period of the forcing function, and again multiply Eq. (50) by $\cos(c\Omega\tau)$ and integrate it over one period of the forcing function) leads to following two coupled nonlinear algebraic equations defining the relation between the unknown phase ϕ, amplitude of motion A and forcing frequency ratio Ω of the steady state response:

$$(1-c^2\Omega^2)A+\frac{3\beta_2 A^3}{4} = F\cos(\phi) \tag{51}$$

$$\left(\frac{8}{3\pi}\right)(c^2\Omega^2\beta_1 A^2-c^4\Omega^4\beta_3 A^3) = F\sin(\phi) \tag{52}$$

Eliminating the unknown phase ϕ by squaring and adding Eqs. (51) and (52), leads to following steady state amplitude–frequency relation

$$\left(\frac{9\beta_2^2}{16\pi^2}\right)a^3+\left[1.5\beta_2(1-\lambda)+\frac{64\lambda^2}{9\pi^2}(\beta_1^2-2\beta_1\beta_3\lambda+\beta_3^2\lambda^2)\right]a^2+(1-2\lambda)a-F^2 = 0 \tag{53}$$

where $a=A^2$ and $\lambda=\Omega^2$. For given values of the micropump physical parameters and motion amplitude a Eq. (52) is in this work solved numerically for real positive roots a using a MATLAB root finding function. Samples of the numerical simulation results obtained using Eq. (53) are presented and discussed in the next section.

6. Results and discussion

Eqs. (45) and (53), along with Eqs. (41) and (42) were used to numerically simulate, respectively, the valveless micropump mean output flow rate Q and membrane (plate) steady state frequency response (A–Ω) characteristics over a selected range of the valveless micropump physical parameters. The MATLAB root finder function "roots" was used to find the roots of Eq. (53), and a fourth order Runge–Kutta program with constant integration step size of 0.01 written in MATLAB code was used to solve the reduced nonlinear coupled fluid-plate vibration model given by Eq. (43). The simulation was limited to the case of a square plate with simply supported edges and dynamic deflection that corresponds to the first normal mode; e.g., $\phi(\xi_1, \xi_2)$ takes the form

$$\phi(\xi_1, \xi_2) = \sin(\pi\xi_1)\sin(\pi\xi_2) \tag{54}$$

And the selected system parameters defined in Eq. (41) were varied in the range:$0.01 \le b_1 \le 0.02$, $0.02 \le b_2 \le 0.05$, $0.5 \le b_3 \le 1$, $0.3 \le b_4 0.4$, $0.2 b_5 \le 0.7$, and $0.02 \le b_6 \le 0.5$. Poisson's ratio μ and the diffuser loss coefficient C_d are assumed to be, respectively, 0.25 and 1. It is noted that, the dimensionless geometric nonlinearity coefficient β_2 in the present model Eq. (43) is a constant independent of the system dimensionless parameters b_i, $i=1,2,\ldots,6$, C_d and μ, and is, for the first mode of the present simply supported square plate, equals to 1.5. As indicated before, only the parameter β_3 includes the effect of fluid bulk modulus of elasticity and only when this parameter is set to zero the effect of fluid finite stiffness is assumed to be negligible. However this parameter represents the combined effects of resistive, inertial and fluid stiffness effects, (e.g. see Eqs. (42) and (44)), and it is a function of all of the specified micropump geometric and physical parameters. In other words, the effect of fluid stiffness is determined not only by the fluid stiffness bulk modulus but also by all of the specified micropump geometric and physical parameters.

Examples of the obtained results are shown in Figs. 2–8. Figs. 2 and 3 are examples of the study of the accuracy of the amplitude–frequency response analytical results obtained using the approximate analytical solution in Eq. (53) as compared to those obtained by numerically integrating Eq. (43) and the different qualitative behaviors of the response amplitude and output mean flux with excitation frequency ratio Ω. The results displayed in Fig. 3 show that, depending on the relative values of β_1, β_2 (β_2=1.5=constant, or 0), and β_3 the frequency response curves display distinct behaviors. For example, when the resistive effect is dominant, e.g. when β_1 is large relative to β_3, and $\beta_2=0$, the frequency response curve shows no peak and at a frequency $\Omega \ll 1$ starts a rapid descent from a nearly constant value at low frequency to a zero value at high forcing frequency ratio, (Case(A)). When β_1 is large relative to β_3, and β_2≠0.(*e.g.* β_2=1.5), the response curve, as in the previous case, shows a rapid decent to zero value starting at $\Omega \ll 1$ but also can exhibit a resonance peak at a forcing frequency ratio near $\Omega=1$, (Case (B)). When β_1 is not large relative to β_3, and β_2≠0 the frequency response curve can exhibit a nonlinear resonance behavior similar to that of a classical Duffing oscillator with hardening nonlinearity

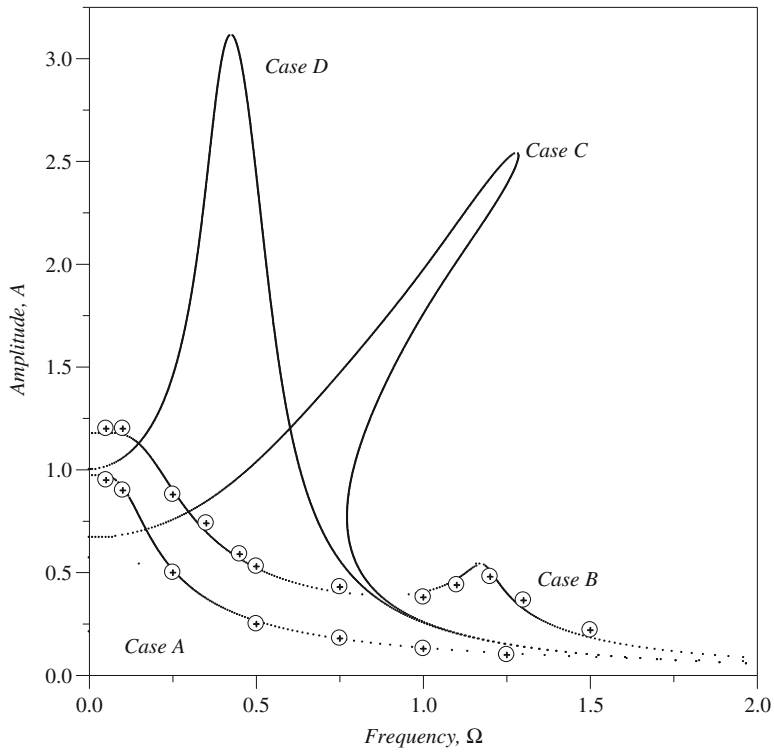

Fig. 2. Frequency response curves Case A; $b_1=0.01$, $b_1=0.04$, $b_3=0.5$, $b_4=0.3$, $b_5=0.5$, $b_6=1$, $C_d=1$, $F=2$, $\beta_1=39.568$, $\beta_2=1.5$, $\beta_3=0.095$. $\oplus$ numerical solution; Case B; $b_1=0.01$, $b_1=0.04$, $b_3=0.8$, $b_4=0.3$, $b_5=0.6$, $b_6=0.03$, $C_d=0.5$, $F=3$, $\beta_1=12.831$, $\beta_2=1.5$, $\beta_3=1.8417$; $\oplus$ numerical solution; Case C; $b_1=0.1$, $b_2=0.04$, $b_3=0.8$, $b_4=0.3$, $b_5=0.6$, $b_6=0.03$, $C_d=0.5$, $F=1$, $\beta_1=0.1283$, $\beta_2=1.5$, $\beta_3=0.01841$; Case D; $b_1=0.1$, $b_2=0.04$, $b_3=0.8$, $b_4=0.3$, $b_5=0.6$, $b_6=0.03$, $C_d=0.5$, $F=1$, $\beta_1=0.1283$, $\beta_2=0$, $\beta_3=0$.

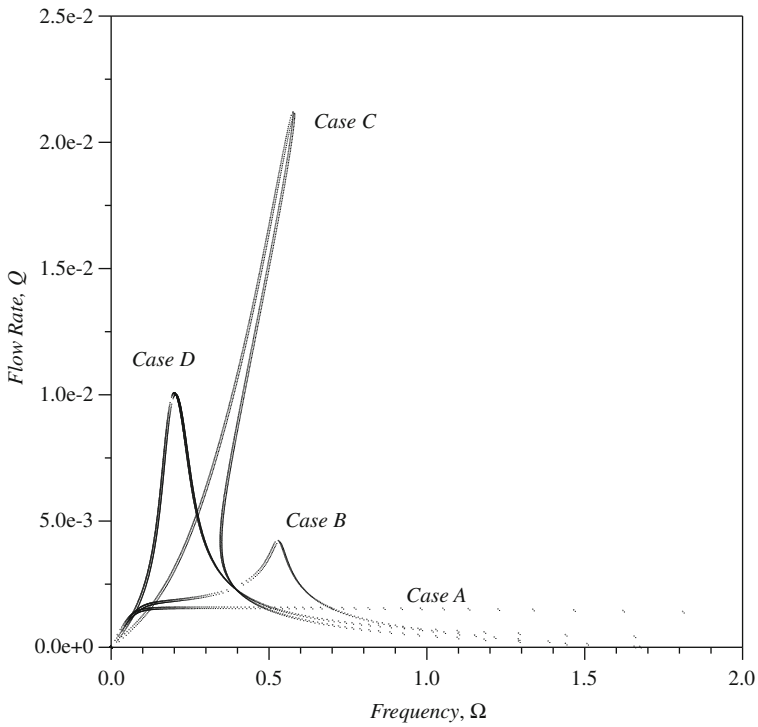

Fig. 3. Mean output flow rate Q for the four cases presented in Fig. 2.

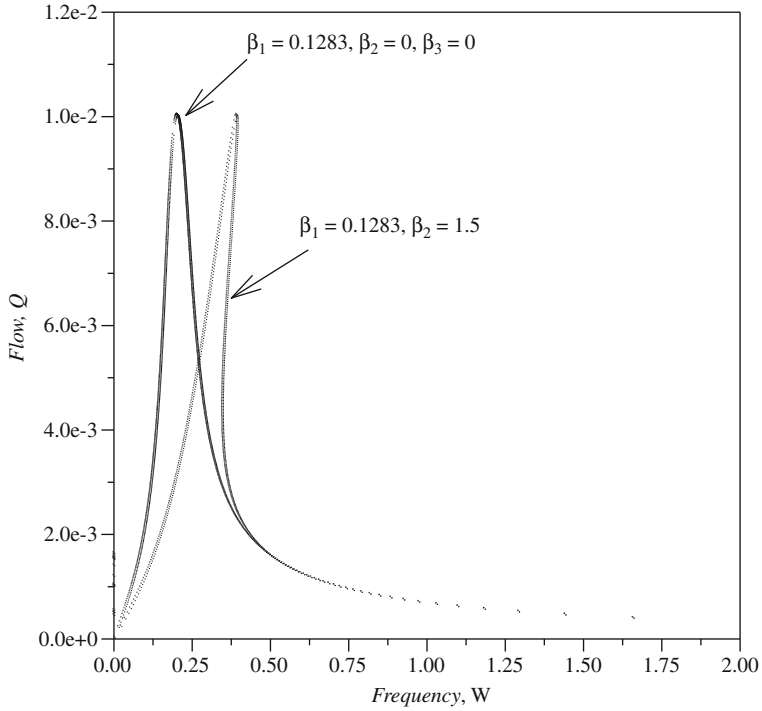

Fig. 4. Effect of structural nonlinearity parameter β_2 on mean output flow rate Q: b_1=0.1, b_2=0.04, b_3=0.8, b_4=0.3, b_5=0.6, b_6=0.03, C_d=0.5, F=1, β_3=0.

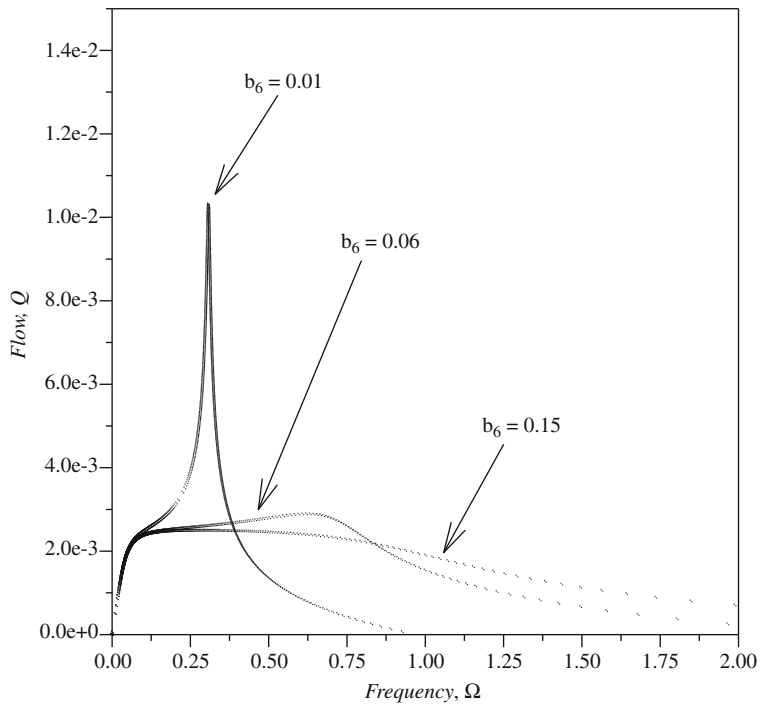

Fig. 5. Effect of fluid stiffness parameter β_3 on mean output flow rate Q b_1=0.01, b_2=0.04, b_3=0.8, b_4=0.3, b_5=0.6, C_d=0.25, F=3. For; b_6=0.01, β_1=6.4159, β_2=0, β_3=0.4604. For b_6=0.15, β_1=6.4159, β_2=0, β_3=0.1842.

(Case(C)). When only resistive and inertial effects are considered, e.g., when β_1≠0, $\beta_2=\beta_3=0$, the frequency response curve, which resembles that of a linear oscillator, exhibits a peak at forcing frequency ratio $\Omega \ll 1$, which agrees qualitatively with the results presented in [16]. The analytical results in this figure show a reasonable agreement with the

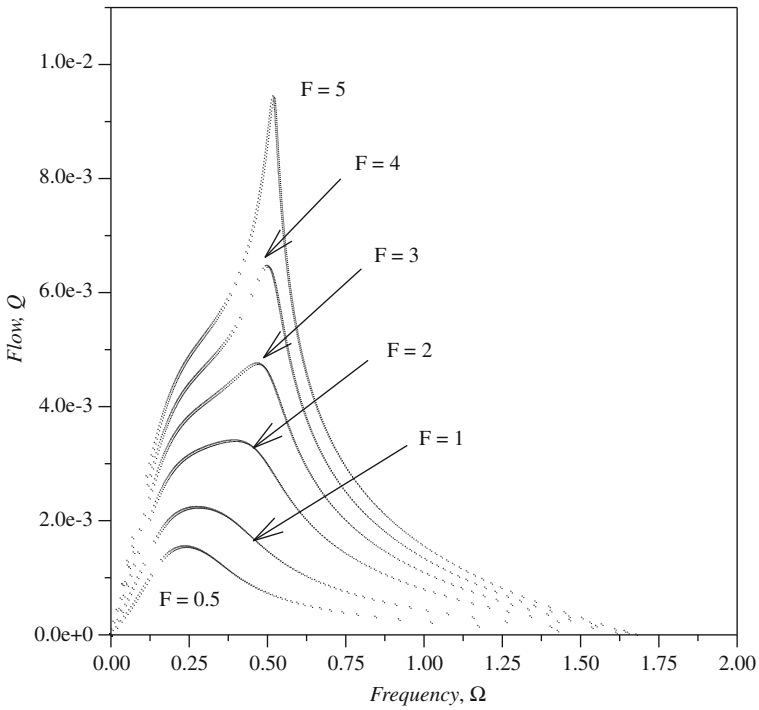

Fig. 6. Effect of excitation level F on mean output flow rate Q b_1=0.02, b_2=0.04, b_3=0.8, b_4=0.3, b_5=0.6, b_6=0.03, C_d=0.5, β_1=3.208, β_2=1.5, β_3=0.4604.

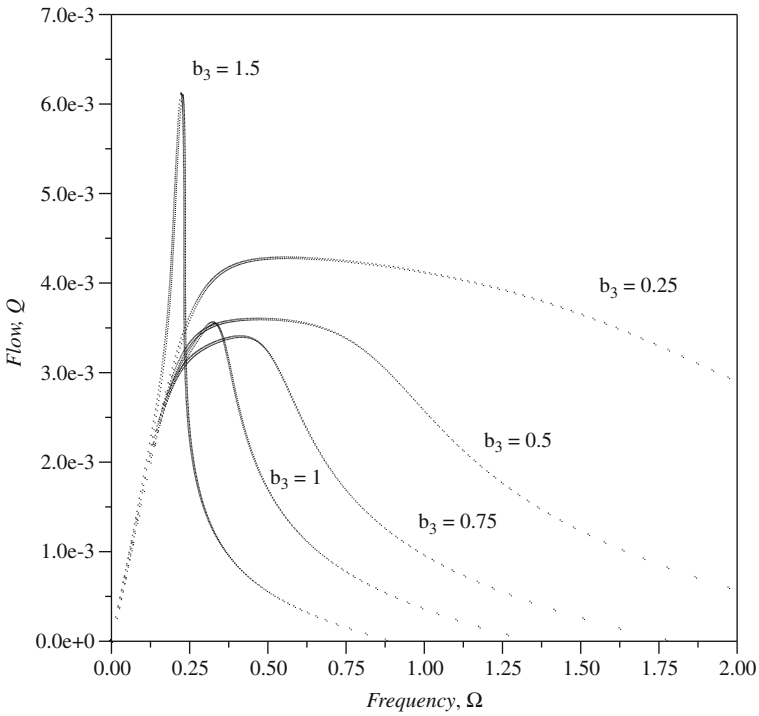

Fig. 7. Effect of b_5=L/a ratio on mean output flow rate Q: b_1=0.02, b_2=0.04, b_4=0.3, b_5=0.6, b_6=0.03, C_d=0.5, F=2 (a) b_3=0.25, β_1=7.1, β_2=1.5, β_3=0.2205; (b) b_3=0.50, β_1=4.57, β_2=1.5, β_3=0.3661; (c) b_3=0.75, β_1=3.376, β_2=1.5, β_3=0.448; (d) b_3=1.0, β_1=2.674, β_2=1.5, β_3=0.50; (e) b_3=1.5, β_1=1.889, β_2=1.5, β_3=0.5614.

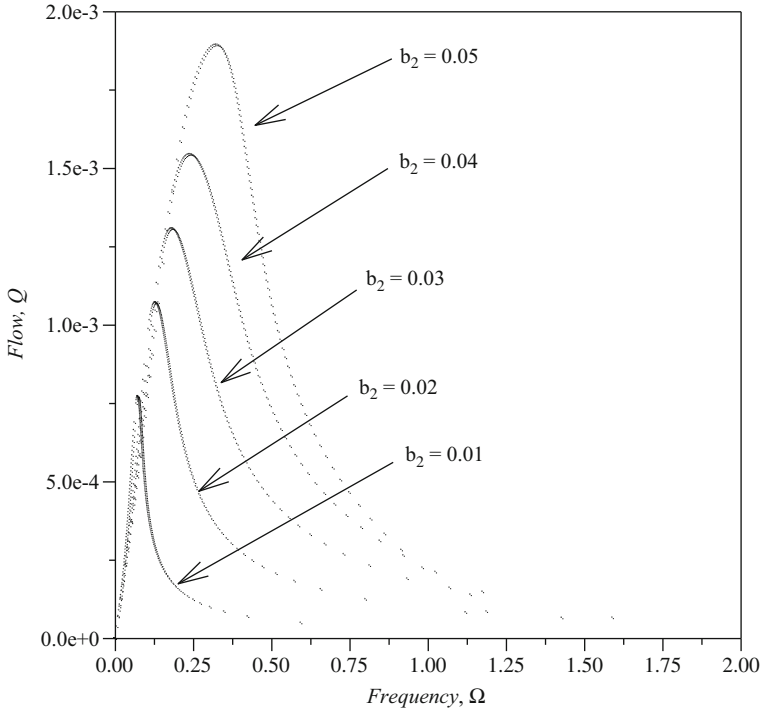

Fig. 8. Effect of $b_2=h/a$ ratio on mean output flow rate Q: $b_1=0.02$, $b_3=0.7$, $b_4=0.3$, $b_5=0.6$, $b_6=0.03$, $C_d=0.5$, $F=0.5$ (a) $b_2=0.01$, $\beta_1=0.945$, $\beta_2=1.5$, $\beta_3=0.0025$; (b) $b_2=0.02$, $\beta_1=1.784$, $\beta_2=1.5$, $\beta_3=0.0356$; (c) $b_2=0.03$, $\beta_1=2.536$, $\beta_2=1.5$, $\beta_3=0.1616$, (d) $b_2=0.04$, $\beta_1=3.208$, $\beta_2=1.5$, $\beta_3=0.460$, (e) $b_2=0.05$, $\beta_1=3.817$, $\beta_2=1.5$, $\beta_3=1.0184$.

numerical results shown for some points on some of these curves. It is noted that the numerical solution, as one may expect for such a highly nonlinear third order system, is not an easy task and was found to be highly sensitive to initial conditions. In particular, numerical verification of the results corresponding to Case (C) in Fig. 2 was not possible and it is not clear weather this is due to instability of the obtained analytical results which was not carried out in this work due to scope limitations, or is due to accuracy limitations of the used numerical procedure.

Fig. 3 displays the mean flux output Q corresponding to cases considered in Fig. 2. The results in this figure also show that, depending on the relative values of β_1, $\beta_2$and β_3, the output mean flux variation with Ω can exhibit distinct qualitative behaviors. In each case, Q starts from a zero value at zero Ω, then follows a curve that is qualitatively similar to corresponding amplitude–frequency response one. Also these results show a characteristic property of valveless micropumps [16,18] that the ratio Ω of the excitation frequency to dry plate natural frequency at which Q attains a maximum value, termed as the optimal operating frequency ratio, is less than that at which the plate deflection is maximum. As noted before, for the case $\beta_2=\beta_3=0$, the present model reduces to that in [18] and the present results in Fig. 3 for this case show a similar qualitative behavior as that of the results reported in [18] which show that the Q attains a maximum value at $\Omega \ll 1$ and falls rapidly to a zero values as Ω is continuously increased above this optimal Ω value. When β_3 and/or $\beta_2$are not zero, the value of the optimal operating frequency and the rate at which Q falls to zero as Ω is increased above the optimal value of Ω depend on the relative values of β_1, β_2 and β_3, Examples of different behaviors of Q–Ω curves for different values of β_1, β_2 and β_3 corresponding to selected values of the micropump and working fluid physical parameters are displayed in Figs. 4–8. These results indicate that working fluid stiffness as well as the actuating membrane geometric structural nonlinearity can have a significant effect on the predicted micropump output mean flux Q behavior with excitation frequency. The present results also show the dynamic performance of micropump is strongly dependent on the relative size of its internal elements. Finally, these results indicate that, (see Fig. 7), Q tends to increase moronically with excitation amplitude, thus from control point of view the excitation amplitude can provide a valuable mean to control the micro-pump output flux.

7. Conclusion

A reduced third order nonlinear single mode model which accounts, in a simplified form, for the plate geometric nonlinearity due to induced in-plane membrane force and the working fluid finite stiffness, is developed and used to simulate the dynamic behavior of a valveless micropump under simple harmonic excitation for the case of equal inlet and outlet pressures and simply supported plate boundary conditions. The present study results indicate that working fluid

stiffness and the actuating plate structural nonlinearity, can have, depending on the micropump geometric and physical parameters, significant effects on the pump dynamic response characteristics. The low order approximate analytical solution for the present third order model showed a reasonably good agreement with those obtained numerically for cases for which the amplitude–frequency response did not exhibit a strong nonlinear resonance behavior. Stability analysis of obtained approximate analytical solution and/or the use of an efficient numerical method are required to analyze the cases of strong nonlinear resonance response and such a task is considered beyond the intended scope of the present work. Also the preset single mode model, as well as those available in the open literature, is based on an initially perfectly flat plate, uniform simple supported or clamped boundary conditions and linear self similar dynamic deflection mode shapes. The present model and results show that the micropump can exhibit a complex nonlinear dynamic behavior which cannot be uncovered by a simplified model and a simplified analysis. It is noted that experimental and/or numerical validations of the obtained approximate analytical model and results are required. Also the investigation of other possible boundary conditions, and the usage of more than one-mode shape and/or other methods to discretize the governing nonlinear continuous field equations can give more insight into the dynamic performance of the considered valveless micropump. Because of scope limitations a numerical validation of the obtained approximate analytical model is considered in a future investigation.

References

[1] D.J. Laser, J.G. Santiago, A review of micropumps, *Journal of Micromechanical and Microengineering* 14 (2004) R35–R64.
[2] E. Stemme, G. Stemme, A valveless diffuser/nozzle-based fluid pump, *Sensors and Actuators A* 39 (1993) 159–167.
[3] A. Olsson, E. Stemme, G. Stemme, A valve-less planar fluid pump with two pump chambers, *Sensors and Actuators A* 46–47 (1995) 549–556.
[4] T. Gerlach, H. Wurmus, Working principle and performance of the dynamic micropump, *Sensors and Actuators, A* 50 (1995) 135–140.
[5] A. Ullman, The piezoelectric valveless pump-performance enhancement analysis, *Sensors and Actuators A* 50 (1998) 97–105.
[6] T. Gerlach, Microdiffusers as dynamic passive valves for micropump applications, *Sensors and Actuators A* 69 (1998) 181–191.
[7] X.N. Jiang, Z.Y. Zhou, X.Y. Huang, Y. Li, Y. Yang, C.Y. Liu, Micronozzle/diffuser flow and its application in micro valveless pumps, *Sensors and Actuators A* 70 (1998) 81–87.
[8] A. Olsson, G. Stemme, E. Stemme, Numerical and experimental studies of flat-walled diffuser elements for valveless micropumps, *Sensors and Actuators A* 84 (2000) 165–175.
[9] K.S. Young, I.Y. Chen, C.C. Wang, Investigation of the flow characteristics within a micronozzle/diffuser, *Journal of Micromechanics and Microengineering* 14 (2003) 26–31.
[10] V. Singhal, S.V. Garimella, J.Y. Murthy, Low Reynolds number flow through nozzle-diffuser elements in valveless micropumps, *Sensors and Actuators A* 113 (2004) 226–236.
[11] M.T. Ahmadian, A. Mehrabian, Design optimization by numerical characterization of fluid flow through the valveless diffuser micropumps, *Journal of Physics: Conference Series* 34 (2006) 379–384.
[12] Q.-L. Zhao, J. Yuan, H.-M. Liu, Z.-X. Duan, Stationary fluid dynamic behavior of V-shaped diffuser/nozzle elements for valveless micropumps, *Chinese Physics Letters* 25 (4) (2008) 1359–1361.
[13] Q. Cui, C. Liu, X.F. Zha, Study of a piezoelectric micropump for the controlled drug delivery system, *Microfluid Nanofluid* 3 (2007) 377–390.
[14] T.Y. Ng, T.Y. Jiang, H. Li, K.Y. Lam, J.N. Reddy, A coupled field study on the non-linear characteristics of an electrostatic micropump, *Journal of Sound and Vibration* 273 (2004) 989–1006.
[15] A. Olsson, G. Stemme, E. Stemme, A numerical study of the valveless diffuser pump using a lumped-mass model, *Journal of Micromechanics and Microengineering* 9 (1999) 34–44.
[16] L.S. Pan, T.Y. Ng, G.R. Liu, K.Y. Lam, T.Y. Jiang, Analytical solutions for the dynamic analysis of a valveless micropump—a fluid–membrane coupling study, *Sensors and Actuators, A* 93 (2001) 173–181.
[17] A. Machauf (Prochaska), Y. Nemirosky, U. Dinnar, A membrane micropump electrostatically actuated across the working fluid, *Journal of Micromechanics and Microengineering* 15 (2005) 2309–2316.
[18] L.S. Pan, T.Y. Ng, X.H. Wu, H.P. Lee, Analysis of valveless micropumps with inertial effects, *Journal of Micromechanics and Microengineering* 13 (2003) 390–399.
[19] B. Fan, G. Song, F. Hussain, Simulation of a piezoelectrically actuated valveless micropump, *Smart Materials and Structures* 14 (2005) 400–405.
[20] H.M. Berger, A new approach to the analysis of large deflections of plates, *Journal of Applied Mechanics* 22 (1995) 465–472.
[21] T. Wah, Large amplitude flexural vibrations of rectangular plates, *International Journal of Mechanical Sciences* 5 (1963) 425–434.
[22] J. Ramachandran, D.V. Reddy, Nonlinear vibrations of rectangular plates with cutouts, *AIAA Journal* 10 (1972) 709–710.
[23] A.H. Nayfeh, M.J. Younis, E.M. Abdel-Rahman, Reduced-order models for MEMS applications, *Nonlinear Dynamics* 41 (2005) 211–236.
[24] J.G. Eisley, Nonlinear vibrations of beams and rectangular plates, *ZAMP* 15 (1964) 167–175.
[25] C.-Y. Chia, *Nonlinear Analysis of Plates*, McGraw-Hill, New York, 1980.
[26] A.H. Nayfeh, D.T. Mook, *Nonlinear Oscillations*, John Wiley, New York, 1979.
[27] D.W. Jordan, P. Smith, *Nonlinear Ordinary Differential Equations*, Oxford University Press, Oxford, 1977.